Comparison of Nonequilibrium Viscous-Shock-Layer Solutions with Shuttle Heating Measurements

R. A. Thompson*
NASA Langley Research Center, Hampton, Virginia

A three-dimensional viscous-shock-layer code has been modified and used to compute the nonequilibrium flowfield over the windward surface of the Space Shuttle Orbiter for re-entry conditions between 75 and 60 km. Centerline heating predictions obtained with the modified code using a recent expression for oxygen recombination at the Shuttle surface were found to be in good agreement with flight data from STS-2 and STS-3. The centerline predictions also show a roughly 30% decrease in heat transfer in comparison with previous results and are now in agreement with two-dimensional viscous-shock-layer results. Comparisons of heating predictions on the off-centerline windward surface were in good agreement with the data flight, and the calculated results followed measured trends in the crossflow heating distributions.

Nomenclature

C_i = mass fraction of species i, ρ_i/ρ
C_p = frozen specific heat of mixture, $\Sigma_i C_i C_{p,i}$
$C_{p,i}$ = specific heat of species i, $C^*_{p,i}/C^*_{p,\infty}$
D_{ij} = binary diffusion coefficients
g = determinant of the metric tensor
$\bar{g}_i$ = vector in the ξ_i direction
$\bar{g}^i$ = vector orthogonal to $\bar{g}_j$ and $\bar{g}_k$, $i \neq j$, $i \neq k$
g_{ij} = coordinate metric tensor, $\bar{g}_i \cdot \bar{g}_j$, $i,j = 1,2,3$
g^{ij} = $\bar{g}_i \cdot \bar{g}^j$, $i,j = 1,2,3$
h = enthalpy of mixture, $\Sigma_i C_i h_i$
h_i = enthalpy of species i, h^*_i/U^{*2}_∞
K = thermal conductivity of mixture, $K^*/\mu^*_{\text{ref}} C^*_{p,\infty}$
k^*_w = surface catalytic recombination rate
L = vehicle length measured along x coordinate
Le = Lewis number, $\rho^* D^*_{ij} C^*_p/K^*$
$\bar{M}^*$ = molecular weight of mixture
M^*_i = molecular weight of species i
M_∞ = freestream Mach number
N_S = number of reacting species
n_{sh} = shock standoff distance, n^*_{sh}/R^*_N
Pr = Prandtl number, $\mu^* C^*_p/K^*$
p = pressure, $p^*/\rho^*_\infty U^{*2}_\infty$
$\dot{q}_w$ = wall heat-transfer rate
$\bar{R}^*$ = universal gas constant
R^*_N = nose radius
T = temperature, T^*/T^*_{ref}
T^*_{ref} = reference temperature, $U^{*2}_\infty/C^*_{p,\infty}$
U^*_∞ = freestream velocity
u,v,w = streamwise, normal, and crossflow velocity components nondimensionalized by the freestream velocity
$\dot{w}_i$ = mass rate of formation of species i, $\dot{w}^*_i R^*_N/\rho^*_\infty U^*_\infty$
x,y = axial and spanwise coordinates
α = angle of attack
γ_i = catalytic recombination coefficient
ε = Reynolds number parameter, $\varepsilon^2 = \mu^*_{\text{ref}}/\rho^*_\infty U^*_\infty R^*_N$
μ = viscosity of mixture, μ^*/μ^*_{ref}
μ_{ref} = reference viscosity, $\mu^*(T^*_{\text{ref}})$
ξ_i = nonorthogonal coordinates nondimensionalized by R^*_N, $i = 1,2,3$
ρ = density of mixture, ρ^*/ρ^*_∞

$\left\{ \begin{matrix} i \\ jk \end{matrix} \right\}$ = Christoffel symbol of the second kind, $i,j,k = 1,2,3$

$$\frac{1}{2}\sum_{m=1}^{3} g^{im}\left[\frac{\partial g_{mk}}{\partial \xi_j} + \frac{\partial g_{mj}}{\partial \xi_k} - \frac{\partial g_{jk}}{\partial \xi_m}\right]$$

Subscripts

i = ith species
sh = shock value
w = wall value
∞ = freestream condition

Superscripts

$*$ = dimensional quality

Introduction

PREFLIGHT predictions[1–4] of the aerothermal environment about the Space Shuttle Orbiter indicated possible influences of nonequilibrium flow chemistry. Subsequent temperature and pressure measurements made on the Orbiter during re-entry have provided an extensive and reliable data base to assess and improve those predictions and to enhance understanding of the flow phenomena. Qualitative and quantitative analyses[5–10] of the flight data have demonstrated the low catalytic characteristics of the Shuttle tiles and the attendant decrease in heat transfer relative to predicted equilibrium levels. The calculated results were based on finite-rate chemically reacting boundary-layer and viscous-shock-layer (VSL) methods.[5–8] Flight data from the catalytic surface experiments (CSE)[9,10] have verified that the lower heating rates can be attributed to the fairly noncatalytic nature of the thermal protection system (TPS) and not to unknowns in the freestream or flowfield quantities and that nonequilibrium effects persist to approximately 50 km for the Orbiter.

Computational analyses of the nonequilibrium flow over the Shuttle to date can be classified into three areas. First, boundary-layer and matched inviscid techniques such as those used by Rakich and Lanfranco[1] and Scott[2] have been used to

Presented as Paper 87-1473 at the AIAA 22nd Thermophysics Conference, Honolulu, HI, June 8–10, 1987; received April 6, 1988; revision received Sept. 15, 1988.

*Aerospace Technologist, Aerothermodynamics Branch, Space Systems Division. Member AIAA.

compute streamlines and heating over the forward portion of the windward surface. Second, flowfield analyses have been performed using two-dimensional VSL methods. These investigations used "equivalent" axisymmetric body or "equivalent" hyperboloid geometries to model the windward centerline of the Shuttle Orbiter at high angles of attack. Miner and Lewis[3] used this approach for preflight predictions of surface heating and pressure and shock-layer species profiles. Shinn et al.[5] employed a two-dimensional VSL technique to anlayze the measured STS-2 heat-transfer data. The final group of nonequilibrium computational analyses includes the three-dimensional viscous-shock-layer method developed by Kim et al.[6,7] In this method, the complete lower surface of the Orbiter vehicle is modeled to enable the computation of the windward three-dimensional flowfield.

In all of these studies, the effects of nonequilibrium chemistry on surface heating have been stressed, and important contributions to understanding the measured data and evaluating the computational predictions have been made. Scott[8] has reviewed most of the nonequilibrium techniques and has compiled comparisons of predicted results with data over the altitude range for Shuttle entry. Those comparisons showed differences in heating predictions of 10–30 % depending on body location, altitude, and assumed catalytic efficiency of the surface. Scott also concluded that no one method could adequately predict the heating rates over the entire windward centerline for all conditions. Further work in this area is obviously important for improved understanding of nonequilibrium flows and for increasing confidence in prediction techniques that may be used to design future hypersonic vehicles.

The VSL code of Ref. 6 (SHTNEQ) is currently the only known viscous code to compute the nonequilibrium flowfield over the Shuttle windward surface at angle of attack, and investigations using this code have been reported.[6,7,11] This nonequilibrium code and a similar version (VSL81),[12] which solved the perfect-gas and equilibrium-air flowfields over the Orbiter, have been delivered to NASA Langley Research Center. An effort was initiated to gain a thorough understanding of the codes for possible application to future missions. However, work with the VSL81 code revealed several problems and required significant modification. With these modifications, the code was redesignated VSL84, and the improved capability of the code to predict windward-centerline heating rates on the Shuttle Orbiter demonstrated.[13] Similar improvements as well as additional modifications have recently been made to the SHTNEQ code.

A primary objective of the present paper is to illustrate the effects of the modifications to the SHTNEQ code and to compare the present heat-transfer predictions with experimental data from Shuttle re-entry. Also, the present study assesses the capability of the modified code to predict off-centerline heating distributions and the effects of different oxygen-wall recombination coefficients on the predicted heat transfer.

Analysis

Viscous-shock-layer theory has been widely used over the last decade for numerical solution of hypersonic flows over a range of body shapes and freestream conditions. Because of the simplicity of the technique, many physical models have been incorporated into VSL codes for further in-depth study or detailed flowfield calculations.[14–18] The VSL equations are a subset of the Navier-Stokes equations wherein parabolic approximations have been made in the streamwise and crossflow directions. Thus, the equations can be solved by marching techniques that are efficient in terms of computer time and storage requirements. The VSL equations are easier to apply than matched boundary-layer and inviscid solutions since no coupling problems exist (e.g., entropy layer swallowing) between inviscid and viscous regions. The equations are limited, however, to attached flow in both the streamwise and crossflow directions, unlike some higher approximations.

Governing Equations

The VSL equations are derived from the steady-state Navier-Stokes equations for a reacting gas mixture[18] written in general tensor form. Some terms are dropped in the current formulation because of the nonorthogonal, body-normal coordinate system,[19] and the resulting equations are nondimensionalized for an order-of-magnitude analysis. For the VSL approximation, the normal velocity and normal coordinate are assumed to be of order ε, where ε is the inverse square root of the Reynolds number parameter. All terms of order ε or less are retained, and all higher-order terms are neglected. Also, all viscous terms in the normal momentum equation are dropped so that the normal momentum, global continuity, and species continuity equations are first order, whereas the remaining equations are second order.

The VSL equations are presented, herein, with u,v,w as the tensor velocity components. This set includes additional viscous terms in the axial momentum, crossflow momentum, and energy equations which were neglected in the original derivation. The global continuity and momentum equations are identical to the equations given in Ref. 13, but the energy equation includes the chemical production and diffusion terms to account for the finite-rate chemistry. Also, species conservation equations are included to describe the reacting gas. The equations are as follows:

Continuity:

$$\frac{\partial}{\partial\xi_1}(\rho u\sqrt{g})+\frac{\partial}{\partial\xi_2}(\rho v\sqrt{g})+\frac{\partial}{\partial\xi_3}(\rho w\sqrt{g})=0 \tag{1}$$

ξ_1 momentum:

$$\rho u\frac{\partial u}{\partial\xi_1}+\rho v\frac{\partial u}{\partial\xi_2}+\rho w\frac{\partial u}{\partial\xi_3}+\rho\left[u^2\begin{Bmatrix}1\\11\end{Bmatrix}+2uv\begin{Bmatrix}1\\12\end{Bmatrix}+2uw\begin{Bmatrix}1\\13\end{Bmatrix}+v^2\begin{Bmatrix}1\\22\end{Bmatrix}+2vw\begin{Bmatrix}1\\23\end{Bmatrix}+w^2\begin{Bmatrix}1\\33\end{Bmatrix}\right]+\frac{1}{g}\left[g_{33}\frac{\partial p}{\partial\xi_1}-g_{13}\frac{\partial p}{\partial\xi_3}\right]$$
$$=\varepsilon^2\left[\frac{\partial\mu}{\partial\xi_2}\frac{\partial u}{\partial\xi_2}+\mu\frac{\partial^2 u}{\partial\xi_2^2}\right]+\mu\varepsilon^2\left[3\frac{\partial u}{\partial\xi_2}\begin{Bmatrix}1\\21\end{Bmatrix}+\frac{\partial u}{\partial\xi_2}\begin{Bmatrix}3\\23\end{Bmatrix}+2\frac{\partial w}{\partial\xi_2}\begin{Bmatrix}1\\23\end{Bmatrix}\right] \tag{2}$$

ξ_2 momentum:

$$\rho u\frac{\partial v}{\partial\xi_1}+\rho v\frac{\partial v}{\partial\xi_2}+\rho w\frac{\partial v}{\partial\xi_3}+\rho\left[u^2\begin{Bmatrix}2\\11\end{Bmatrix}+2uv\begin{Bmatrix}2\\12\end{Bmatrix}+2uw\begin{Bmatrix}2\\13\end{Bmatrix}+v^2\begin{Bmatrix}2\\22\end{Bmatrix}+2vw\begin{Bmatrix}2\\23\end{Bmatrix}+w^2\begin{Bmatrix}2\\33\end{Bmatrix}\right]+\frac{\partial p}{\partial\xi_2}=0 \tag{3}$$

ξ_3 momentum:

$$\rho u\frac{\partial w}{\partial\xi_1}+\rho v\frac{\partial w}{\partial\xi_2}+\rho w\frac{\partial w}{\partial\xi_3}+\rho\left[u^2\begin{Bmatrix}3\\11\end{Bmatrix}+2uv\begin{Bmatrix}3\\12\end{Bmatrix}+2uw\begin{Bmatrix}3\\13\end{Bmatrix}+v^2\begin{Bmatrix}3\\22\end{Bmatrix}+2vw\begin{Bmatrix}3\\23\end{Bmatrix}+w^2\begin{Bmatrix}3\\33\end{Bmatrix}\right]+\frac{1}{g}\left[g_{11}\frac{\partial p}{\partial\xi_3}-g_{13}\frac{\partial p}{\partial\xi_1}\right]$$
$$=\varepsilon^2\left[\frac{\partial u}{\partial\xi_2}\frac{\partial w}{\partial\xi_2}+\mu\frac{\partial^2 w}{\partial\xi_2^2}\right]+\mu\varepsilon^2\left[\frac{\partial w}{\partial\xi_2}\begin{Bmatrix}1\\21\end{Bmatrix}+2\frac{\partial u}{\partial\xi_2}\begin{Bmatrix}3\\12\end{Bmatrix}+3\frac{\partial w}{\partial\xi_2}\begin{Bmatrix}3\\23\end{Bmatrix}\right] \tag{4}$$

Energy:

$$\rho u C_p \frac{\partial T}{\partial \xi_1} + \rho v C_p \frac{\partial T}{\partial \xi_2} + \rho w C_p \frac{\partial T}{\partial \xi_3} - \left[u \frac{\partial p}{\partial \xi_1} + v \frac{\partial p}{\partial \xi_2} + w \frac{\partial p}{\partial \xi_3} \right]$$
$$= \varepsilon^2 \frac{\partial}{\partial \xi_2}\left(K \frac{\partial T}{\partial \xi_2} \right) + \varepsilon^2 \frac{K}{\sqrt{g}} \frac{\partial \sqrt{g}}{\partial \xi_2} \frac{\partial T}{\partial \xi_2}$$
$$+ \varepsilon^2 \sum_{i=1}^{Ns} C_{p,i} \frac{\mu Le}{Pr} \frac{\partial^{C_i}}{\partial \xi_2} \frac{\partial T}{\partial \xi_2} - \sum_{i=1}^{Ns} h_i \dot{w}_i$$
$$+ \varepsilon^2 \mu \left[g_{11} \left(\frac{\partial u}{\partial \xi_2} \right)^2 + 2 g_{13} \frac{\partial u}{\partial \xi_2} \frac{\partial w}{\partial \xi_2} + g_{33} \left(\frac{\partial w}{\partial \xi_2} \right)^2 \right] \quad (5)$$

Species continuity:

$$\rho u \frac{\partial C_i}{\partial \xi_1} + \rho v \frac{\partial C_i}{\partial \xi_2} + \rho w \frac{\partial C_i}{\partial \xi_3} = \frac{\varepsilon^2}{\sqrt{g}} \frac{\partial}{\partial \xi_2}\left(\sqrt{g} \frac{\mu Le}{Pr} \frac{\partial C_i}{\partial \xi_2} \right) + \dot{w}_i \quad (6)$$

Thermodynamic and Transport Properties

Thermodynamics for the multicomponent air mixture are determined assuming a thermally perfect gas. The equation of state for the gas mixture is given by

$$p = \frac{p \bar{R}^* T}{\bar{M}^* C^*_{p,\infty}} \quad (7)$$

Thermodynamic properties for the individual species are obtained by interpolation in the data of Browne.[20-22] This thermodynamic model follows the formulation of Ref. 3, where more details can be found.

Transport properties for the gas mixture are obtained using the methods of Armaly and Sutton[23] for viscosity and Mason and Saxena[24] for thermal conductivity. Individual species viscosity and the translational components of thermal conductivity are computed from curve fits to the data of Yos.[25] A binary-diffusion model is currently used with the diffusion coefficients determined by setting the Lewis number equal to 1.4. The evaluation of transport properties for this study is different from the methods used in Ref. 6. The species transport properties used herein are based on more recent data of Yos.[25] These data are believed to be more accurate at the higher temperatures that are encountered in nonequilibrium calculations. Also, the current mixture thermal-conductivity relation[24] accounts for the contribution from the internal mode, whereas the relation[26] used in Ref. 6 does not.

Chemical Reaction Model

A seven-species chemical reaction model is employed in the current code and follows the model used by Miner and Lewis.[3] The species production terms appearing in the energy and species continuity equations are written in terms of temperatures and species concentration following the approach of Davis[27] and Blottner et al.[28] The seven reaction equations for the different species (O, O_2, N, N_2, NO, NO^+, e^-) are as follows:

$$O_2 + M1 = 2O + M1$$
$$N_2 + M2 = 2N + M2$$
$$N_2 + N = 2N + N$$
$$NO + M3 = N + O + M3$$
$$NO + O = O_2 + N$$
$$N_2 + O = NO + N$$
$$N + O = NO^+ + e^-$$

Rate constants for the forward and backward reactions and the relative efficiencies of the catalytic third bodies (M1, M2, M3) are obtained from Blottner et al.[28] These rate equations and constants are identical to those used in previous studies.[3,6,7] The first six reactions and associated constants are also identical to those used in two-dimensional VSL studies.[5,29]

Initial and Boundary Conditions

The three-dimensional VSL solution is initiated on a spherical nosecap where an axisymmetric solution in a wind-fixed coordinate system is obtained. The wind-fixed solution extends downstream past the geometric stagnation point where it is then rotated and interpolated to obtain a three-dimensional starting plane in body-fixed coordinates. This method is exact for spherically blunted bodies but is an approximation for the Shuttle geometry. An effective nose radius of 0.62 m (24.5 in.) was used to start the current solutions on the Shuttle geometry.

Shock and wall boundary conditions are prescribed for the VSL solution. Surface temperature is defined using measured data from the Orbiter re-entry. Surface pressure is obtained by one-sided differencing of the normal momentum equation. Wall species concentrations for the present study are determined via finite recombination rates. The boundary condition in this case is calculated by the recombination equation[5] given by

$$\frac{\partial C_i}{\partial \xi_2} - \frac{k_{w_i} \rho Pr}{Le \mu \varepsilon^2} C_i = 0 \quad (8)$$

where the recombination rate k_{w_i} is determined from the recombination coefficient

$$\gamma_i = \sqrt{2\pi M_i^* / \bar{R}^* T^*}\, k^*_{w_i} \quad (9)$$

Recombination-rate expressions of oxygen and nitrogen for the Shuttle TPS were obtained from the experiments by Scott.[4] An additional oxygen recombination expression derived from flight-measured data by Zoby et al.[29] is also considered in the present study. The Shuttle TPS is assumed to be noncatalytic to the recombination of other air species.

Boundary conditions immediately behind the bow shock are computed from the modified shock-jump relations given by Davis[27] for a reacting gas. Production of species across the shock wave is assumed to be zero, and slip conditions are not considered. Initial shock-shape data required to compute the shock-jump conditions are obtained from inviscid solutions using the HALIS code.[30] These data were provided by Mr. K. J. Weilmuenster of the NASA Langley Research Center.

Method of Solution

Numerical solution of the perfect gas and equilibrium air three-dimensional equations has been presented in Refs. 12 and 18. Since solution of the nonequilibrium equations is similar, only an overview is given here. Additional information can be found in Refs. 6 and 7.

The VSL solution begins at the aerodynamic stagnation point by solving the axisymmetric flow over a spherical nosecap as described previously. This axisymmetric solution is rotated and interpolated to provide the three-dimensional starting plane. From this plane, the method "steps" downstream along the windward symmetry place and "marches" around the body until the leeward symmetry plane is reached or until the last leeside plane that can be computed is reached. At each station, the governing equations are solved in a cascading scheme in the following order: species continuity, crossflow momentum, energy, streamwise momentum, integration of global continuity for standoff distance, and the coupled normal momentum and continuity equations. After integration of the continuity equation, the new shock-standoff distance is used to update the shock-layer profile for the next local iteration while the shock slope remains fixed at the input value. The equations are iterated in this manner until each of the flowfield variables is converged through the entire shock layer at the given station.

Global convergence of the VSL solution is satisfied by repeating the calculation over the vehicle using the computed

shock-standoff distances obtained during the previous pass to provide the new shock shape (i.e., standoff distance and slope). Global iterations are continued until the input and output shock shapes are converged. The initial shock shape for the first solution pass (first iteration) is obtained from inviscid equilibrium-air solutions[30] that are scaled by a constant. This scaling factor was determined by numerical experiment with the SHTNEQ code and was in the range of 1.2–1.25 for the current cases. The initial shock shape was treated in this manner to account for nonequilibrium effects in the flowfield and thereby reduce the shock-shape correction and required global iterations. Another reason for this scaling is that the coordinate metrics in the current code are computed once for each global iteration and are not allowed to vary as the computed shock-standoff distances vary with local iterations. In this manner, the metrics are converged in a global sense, and the solution is more consistent if the shock-shape correction is small.

Geometry Model and Finite-Difference Grid

The geometry used to model the Shuttle for the current calculations is a fairly exact representation of the actual windward surface. On the leeside, the true geometry was modified by previous investigators to facilitate the inviscid flowfield calculations.[30] Although the leeside geometry was altered to simplify the flowfield calculation, the overriding point in the geometry definition was that the modified shape should not affect the windward surface flowfield calculations. This modified geometry has been discussed in detail in Ref. 30 and is depicted in Fig. 1.

In the current VSL solutions, 51 points are used between the body and bow shock with clustering of points near the wall. In the ξ_3 direction, the computational planes are spaced at 10-deg intervals at the body surface. The maximum step size in the streamwise direction is limited to 0.5 nose radii. The flowfield solutions obtained herein are limited, on the windward side, to inboard of the Shuttle wing root ($\xi_3 \leq 70$ deg) as shown in Fig. 1, because of the inability to treat the large gradients that occur in that region.

Modifications to the SHTNEQ Code

Although the SHTNEQ code[6] serves as the basis for this study, several modifications have been made in the present work. These modifications are similar to changes made in the perfect-gas and equilibrium-air version of this code that were described in Ref. 13. First, corrections to several terms in the governing equations were made. Terms from the energy and momentum equations required correction because of improper coding and/or incorrect nondimensionalization. Additional viscous-dissipation terms derived from the order-of-magnitude analysis are also retained in the energy, streamwise momentum, and crossflow momentum equations. Probably the most important change is a correction in the evaluation of the shock boundary conditions wherein the proper shock location in the body-normal nonorthogonal coordinate system is now used. This problem previously affected the entire flowfield solution and was reported in Ref. 13 to yield computed shock-standoff distances which were as much as 50% in error. An implicit streamwise pressure gradient is employed in the present work with no difficulty, whereas previous studies[6,7] report using an explict model to promote convergence. For the current calculations, the mixture law for thermal conductivity and the species transport properties are different from those used previously[6,7,11] as described earlier.

Results and Discussion

In this section, the effects of the code modifications on the shock shape and surface heat transfer are demonstrated. The shock convergence for a typical case is illustrated by presenting the results of two solution passes (first and second iterations) for both streamwise and crossflow shock locations. Effects of the modifications on predicted heating rates are demonstrated by comparison of the current results with previous predictions. Afterward, predicted heat-transfer results based on the modified code are compared with STS-2 and STS-3 flight data[31] at four altitudes ranging from approximately 75–60 km. Specific information for these trajectory points is given in Table 1. These later comparisons include symmetry plane and transverse distributions and show the heating effects of different finite-rate oxygen surface recombination expressions.

Effects of Modifications

Shock Convergence

The current flowfield solutions were globally iterated, and the predictions presented herein are from the second solution pass. Figures 2a and 2b illustrate the global convergence of the VSL solution at 71.29 km and are typical of the remaining cases. The first figure (Fig. 2a) shows the output shock-standoff distances along the windward centerline for the first and second solution passes. Figure 2b compares similar cross-sectional shock-shape data. As shown, the output shock shapes from the two iterations are in good agreement which is indicative of the solution convergence. These figures also compare the inviscid perfect-gas and equilibrium-air shock-standoff distances with the nonequilibrium VSL values. Note that the viscous nonequilibrium standoff is between 20–25% greater than the inviscid equilibrium values over most of the windward surface. Similar differences between equilibrium and nonequilibrium standoff distances were also obtained in the two-dimensional solutions of Ref. 5.

An output shock from the second solution pass[7] using the original SHTNEQ code is also presented in Fig. 2a for this case. This nonequilibrium shock is as much as 35% closer to the body than the corresponding inviscid equilibrium shock. Conversely, the current code yields a shock that appears

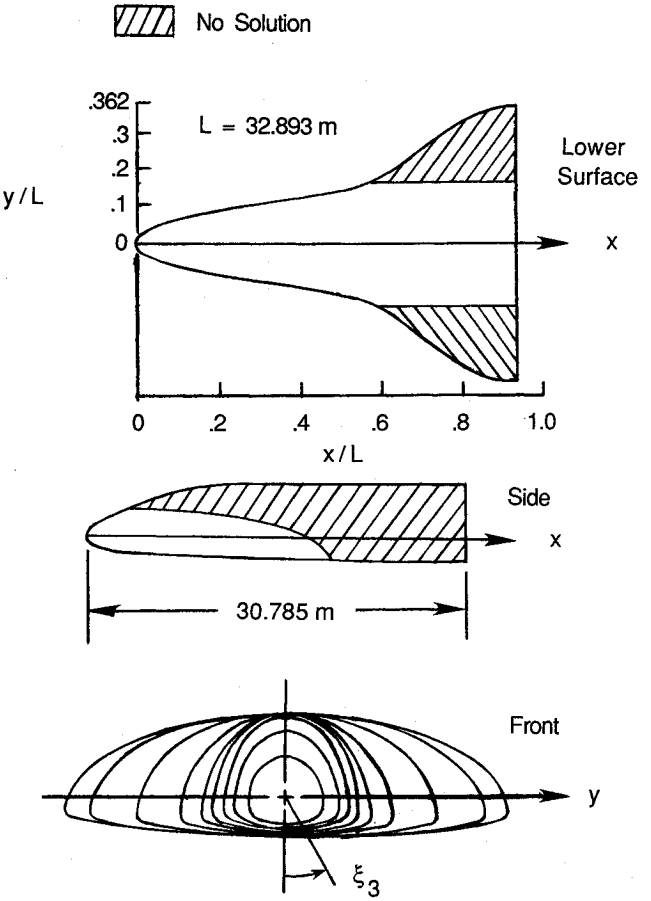

Fig. 1 Geometry of modified Shuttle.

Table 1 Freestream conditions

Flight	Altitude, km	M_∞	α, deg	U_∞, km/s	T_∞, K	P_∞, N/m^2	ρ_∞, kg/m^3
STS-2	74.98	25.0	40.0	7.20	198.0	2.168	3.815×10^{-5}
STS-2	71.29	23.4	39.4	6.73	205.0	4.015	6.824×10^{-5}
STS-3	64.0	17.9	39.3	5.81	262.0	13.997	1.861×10^{-4}
STS-2	60.56	15.7	42.0	4.99	252.8	19.056	2.621×10^{-4}

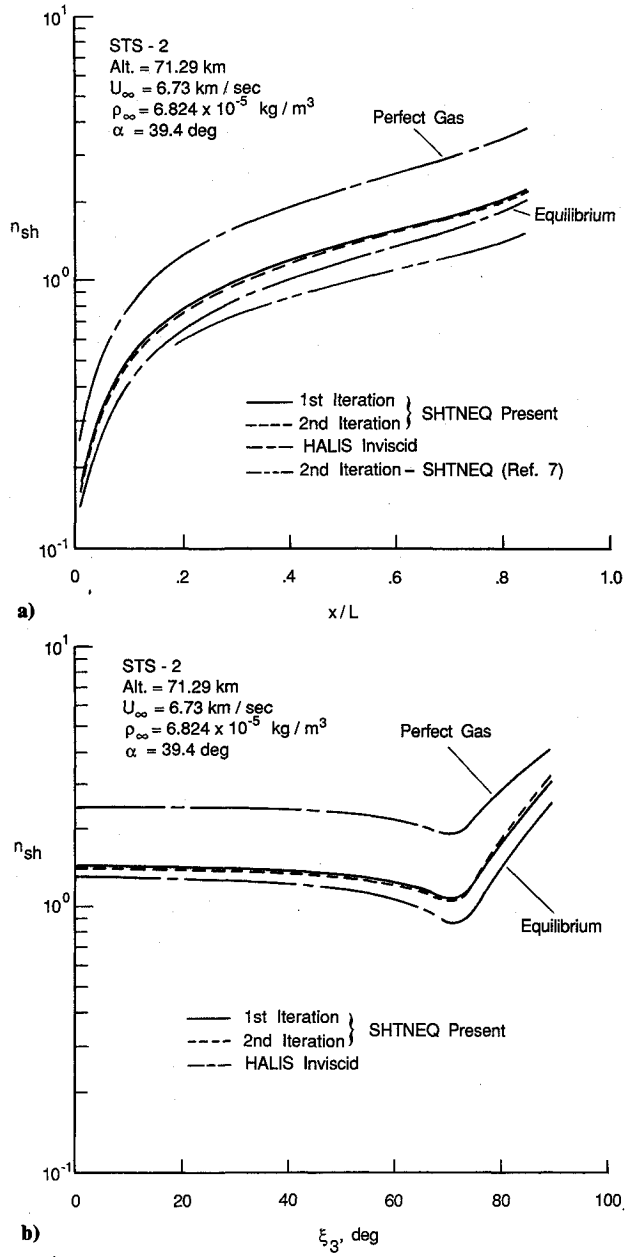

Fig. 2 Shock-shape convergence: a) streamwise, windward centerline; and b) circumferential, $x/L = 0.2$.

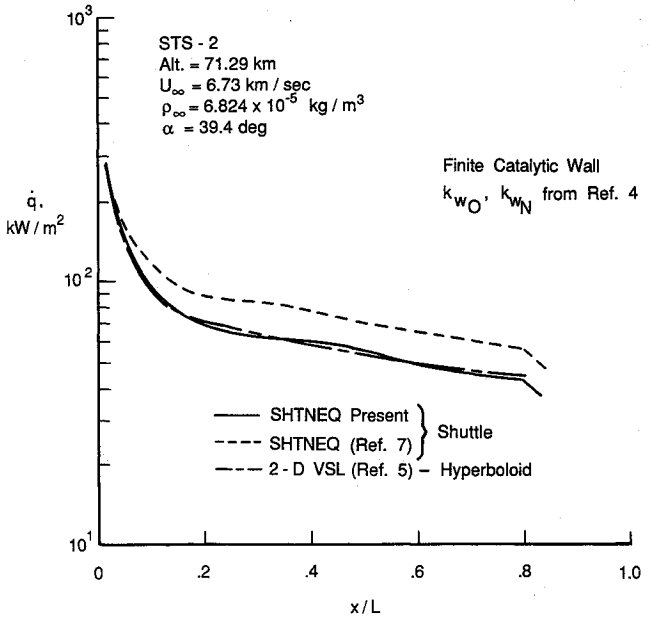

Fig. 3 Comparison of nonequilibrium windward centerline heat-transfer predictions.

qualitatively correct with respect to the perfect-gas and equilibrium-air standoff distances.

Heating Rates

The effects of modifications to the perfect-gas/equilibrium-air version of the three-dimensional VSL code (VSL81) on heat-transfer predictions have been presented in Ref. 13. Those results show that the original code (VSL81) predicts heating rates that are 20–30% greater than those obtained using the modified code (VSL84) and that the new results are in better agreement with Shuttle flight data and other predictions. Similar modifications have since been made to the nonequilibrium SHTNEQ code with the effects shown in Fig. 3, namely, the original code yields heating rates that are 30–40% greater than corresponding values obtained with the modified program. Thus, the modifications to both versions of the three-dimensional VSL Shuttle code are found to have a significant impact on predicted results for both shock shape and surface heat transfer.

Since the three-dimensional VSL code solves the flowfield over the actual Shuttle windward surface, solutions obtained with the method should account for any three-dimensional effects on the heat transfer. Earlier studies[7,11] using the original VSL81 and SHTNEQ codes showed results that indicated significant three-dimensional effects on the heat transfer to the Shuttle windward centerline. It is of interest to re-examine these results, since a large amount of the Shuttle heating data analysis has been performed with two-dimensional VSL codes and any errors introduced into these analyses because of the geometry modeling should be defined.

It was shown in Ref. 13 for the perfect gas/equilibrium cases, and can be seen in Fig. 3 for the nonequilibrium case, that the modified codes (VSL84 and SHTNEQ) predict about the same heating level as other computational methods. These other methods employ equivalent hyperboloids[5,32] and swept-cylinder[33] approximations to model the windward centerline. Predictions using the original three-dimensional VSL codes are higher over most of the Shuttle centerline. These higher heating rates were attributed[7,11] to three-dimensional effects in the case of equilibrium and nonequilibrium chemistry that were not accounted for in the more approximate results. However, based on the results shown in Ref. 13 and Fig. 3, it appears that the primary three-dimensional effect is the shape of the heating distribution (i.e., the inflection around $x/L = 0.5$) and not the magnitude. That is, the approximate solutions agree to within 10–15% with the three-dimensional solutions for perfect gas, equilibrium air, and nonequilibrium

chemistry, and they do not uniformly underpredict the heating rate by 20–30% as reported in Refs. 7 and 11.

Present Nonequilibrium Results

In this section, the results of the current nonequilibrium code are compared with the Shuttle heating data along the windward centerline and on the windward surface in the crossflow direction. Heat-transfer predictions using a single nitrogen recombination-rate expression with two different oxygen surface recombination-rate expressions are presented. The nitrogen recombination rate of Scott[4] is used with his oxygen rate expression and with the oxygen rate expression of Zoby et al.[29] These surface recombination rates correspond to those for the Shuttle tiles. No effort was made to account for the different rates expected in the nose region due to the carbon-carbon nosecap.

Windward Centerline Heat Transfer

Comparisons of the predicted heat-transfer distributions with the Shuttle flight data for the four altitude cases are presented in Figs. 4a–4d for the windward symmetry plane. As shown, the predicted heat-transfer distributions using Zoby's oxygen correlation are generally 15–20% higher than those obtained using Scott's recombination rate. Near the nose, using either oxygen recombination rate yields about the same heating level, which suggests the greater importance of nitrogen recombination in that region. Overall, the agreement between prediction and experiment is better when the oxygen recombination rate of Ref. 29 is used. This is especially true over the forward vehicle surface ($x/L < 0.4$) where the predictions using Zoby's rate in the three-dimensional VSL code are within 10% of the data. Aft of $x/L = 0.4$, the agreement with the flight data is generally not as good. At 74.98 km, the data over the aft end of the vehicle are underpredicted by 20% or more using Zoby's oxygen rate and by more than 30% using the recombination rate of Ref. 4. The data in this case increase slightly as the centerline is transversed with a local peak in heating around 60% of the vehicle length. Flight data from STS-2 and STS-3 at this altitude and above behave similarly. The reasons for this increase in the experimental results and the ability to predict this trend are not yet understood. Possible reasons which have been postulated[8] are

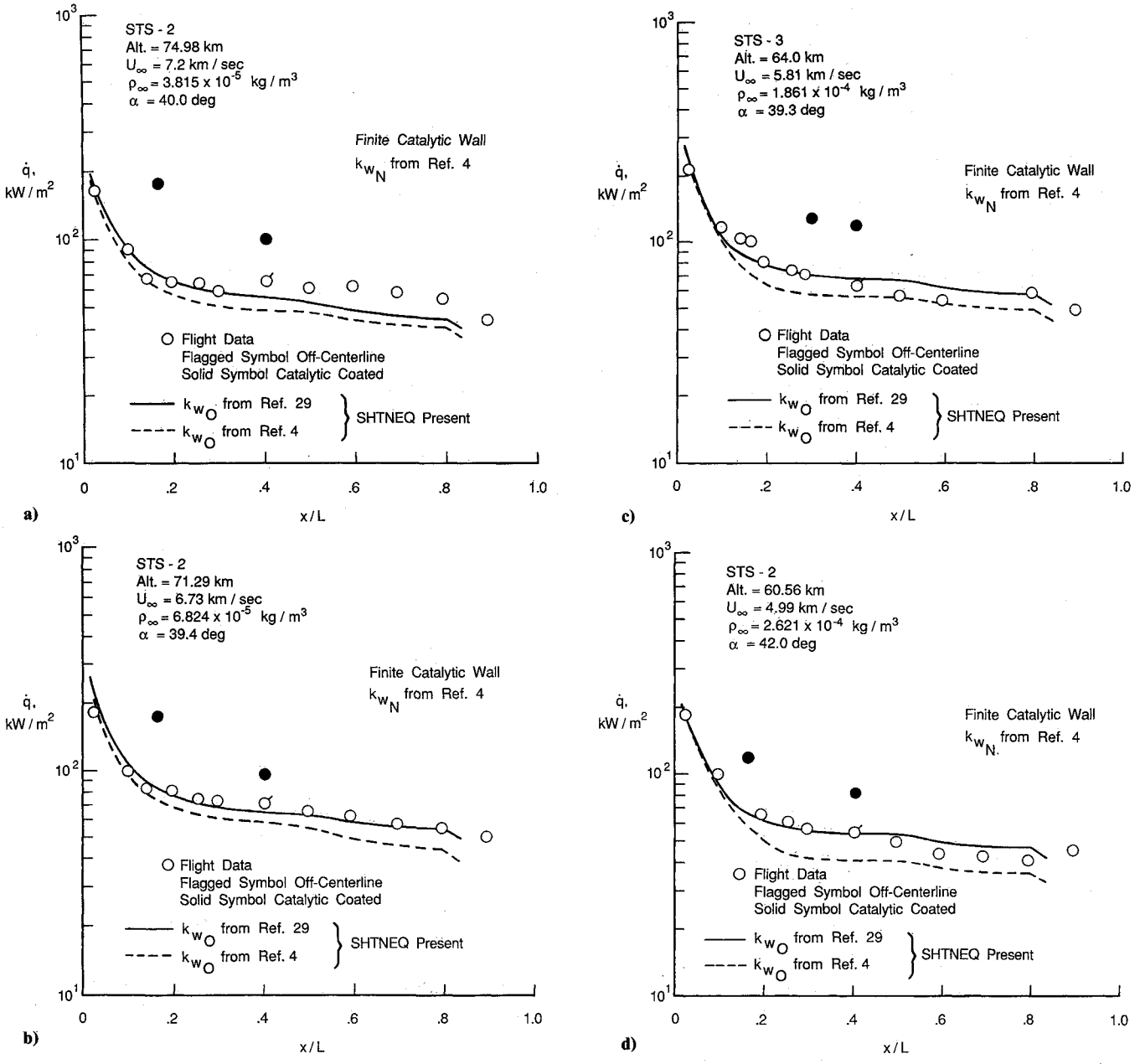

Fig. 4 Nonequilibrium heat-transfer predictions along the windward centerline: a) STS-2, altitude = 74.98 km; b) STS-2, altitude = 71.29 km; c) STS-3, altitude = 64.0 km; and d) STS-2, altitude = 60.56 km.

failure to include adequate modeling of gas-phase reactions and contamination of the aft vehicle surface from tile adhesive or other sources.

At 71.29 km, the prediction using the oxygen recombination rate from Ref. 29 is in excellent agreement with the data over the length of the vehicle (Fig. 4b). The prediction using Scott's rates are again lower over most of the symmetry plane. At lower altitudes (64.0 and 60.56 km), Figs. 4c and 4d show a different trend in the comparison between prediction and experiment than was observed in the first case (74.98 km). In these cases, the predictions with Zoby's expression are in good agreement over the first half of the vehicle but tend to be higher than measured over the aft end. The predictions using Scott's rates are lower over the aft end of the body and agree equally well with the data in that region at these two altitudes.

Windward Surface Heat Transfer

Since the SHTNEQ code solves most of the three-dimensional flowfield over the windward surface, it is of interest to make comparisons between prediction and flight for regions away from the symmetry plane. These comparisons are presented in Figs. 5a–5c for the case at 60.56 km. These figures compare the transverse heating distributions at axial locations (x/L) of 0.098, 0.402, 0.497, 0.592, and 0.691. The predictions shown in these figures are those obtained using the oxygen recombination rate from Ref. 29. The transverse heating levels at each axial station predicted using Scott's recombination rates were lower by an amount equal to the associated centerline prediction and are not shown in these figures.

In general, the heating-rate predictions for the off-centerline data are quite good and are typically within 10–15% of the flight data. Also, the trends of the heating distributions in the crossflow direction are in agreement. The peak in heating occurring at the corner between the lower surface and side fuselage is generally predicted as is the leveling and sometimes decreasing heating rates in the crossflow direction before the heating peak is reached. This latter trend is observed to begin in the computational results for both cases at around $x/L = 0.402$, but it is not clearly seen in the flight data until $x/L \geq 0.592$. At $x/L = 0.497$, prediction of the heating peak is not good in comparison with the flight data and it is believed to be caused by inadequate resolution of the flow in the crossflow direction.

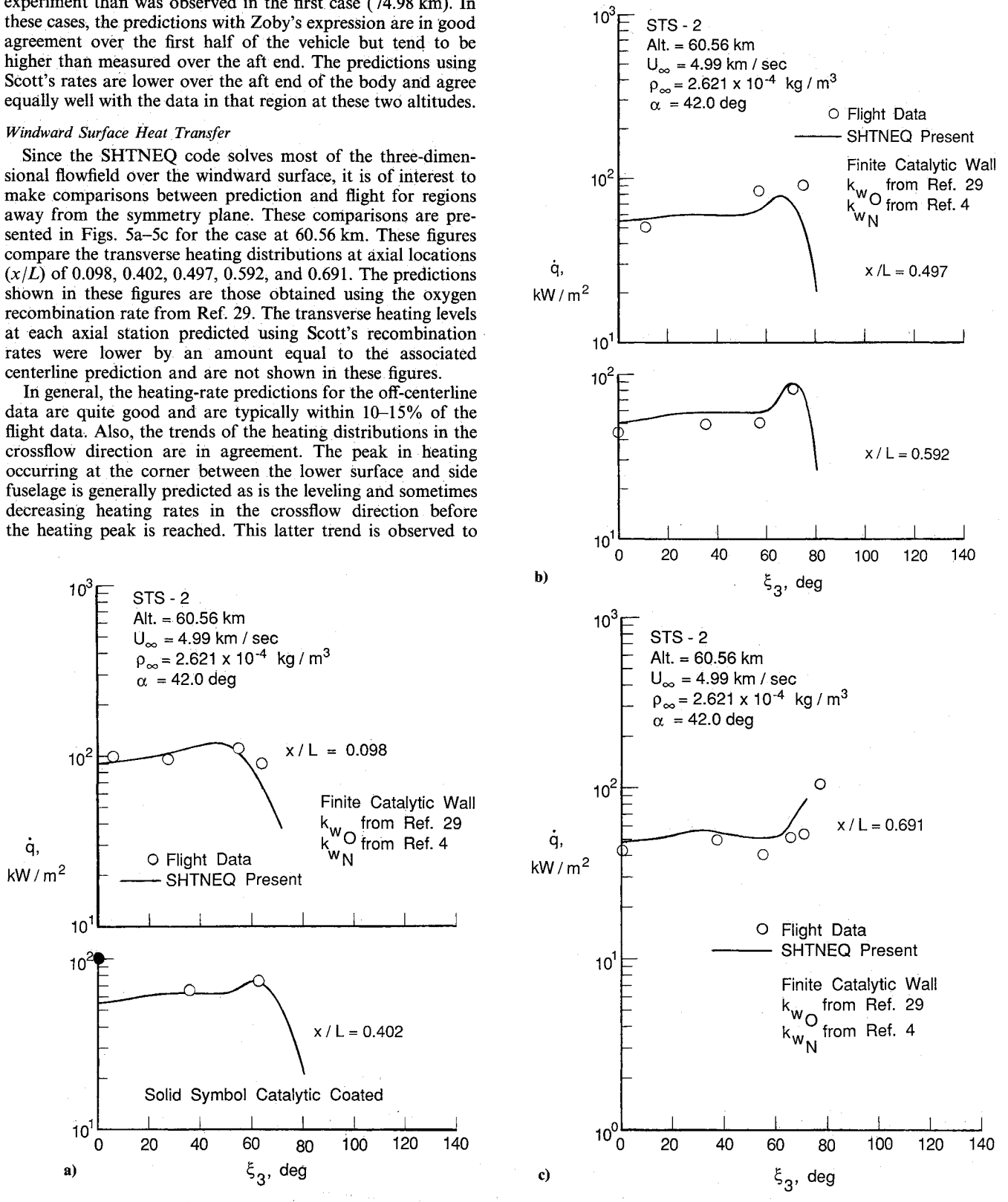

Fig. 5 Nonequilibrium heat-transfer predictions in circumferential direction: a) $x/L = 0.098$, $x/L = 0.402$; b) $x/L = 0.497$, $x/L = 0.592$; and c) $x/L = 0.691$.

Summary

A three-dimensional viscous-shock-layer (VSL) method has been shown to be a viable technique for predicting heating rates over the windward surface of the Shuttle Orbiter under nonequilibrium chemistry conditions. An existing VSL code (SHTNEQ) has been modified, and calculations with the code are compared with flight data, predictions using the original code, and with a two-dimensional VSL prediction that used an equivalent hyperboloid geometry to model the Shuttle windward centerline at angle of attack. In comparisons of the present predictions with windward centerline and off-centerline heat-transfer data, a recent correlation for oxygen surface recombination gave better overall agreement with the flight data than the extrapolation of ground-based experimental recombination data. Predicted centerline and windward surface heat transfer were in good agreement with the flight data, and the predicted trends in heating rates away from the windward symmetry plane appear correct. Previous conclusions about the effects of three-dimensional flow and surface catalysis on heating rates were re-evaluated as a result of recent improvements in the SHTNEQ code. It has been shown in previous work and in current comparisons with the three-dimensional results that the two-dimensional VSL solutions agreed to within 10–15% and were equally accurate for perfect gas, equilibrium, or nonequilibrium chemistries. Future application of the current code for three-dimensional vehicle analyses appears promising based on the verification obtained in this work.

References

[1]Rakich, J. V. and Lanfranco, M. J., "Numerical Computation of Space Shuttle Laminar Heating and Surface Streamlines," *Journal of Spacecraft and Rockets*, Vol. 14, May 1977, pp. 265–272.

[2]Scott, C. D., "Space Shuttle Laminar Heating with Finite-Rate Catalytic Recombination," *Progress in Astronautics and Aeronautics: Thermophysics of Atmospheric Entry*, Vol. 82, edited by T. E. Horton, AIAA, New York, 1982, pp. 273–289.

[3]Miner, E. W. and Lewis, C. H., "Hypersonic Ionizing Air Viscous-Shock-Layer Flows Over Nonanalytical Blunt Bodies," NASA CR-2550, May 1975.

[4]Scott, C. D., "Catalytic Recombination of Oxygen and Nitrogen in High-Temperature Reusable Surface Insulation," *Progress in Astronautics and Aeronautics: Aerothermodynamics and Planetary Entry*, Vol. 77, edited by A. L. Crosbie, AIAA, New York, 1981, pp. 192–212.

[5]Shinn, J. L., Moss, J. N., and Simmonds, A. L., "Viscous-Shock-Layer Heating Analysis for the Shuttle Windward Plane with Surface Finite Catalytic Recombination Rates," AIAA Paper 82-0842, June 1982.

[6]Kim, M. D., Swaminathan, S., and Lewis, C. H., "Three-Dimensional Nonequilibrium Viscous-Shock-Layer Flows Over the Space Shuttle Orbiter," AIAA Paper 83-0487, Jan. 1983.

[7]Kim, M. D., Swaminathan, S., and Lewis, C. H., "Three-Dimensional Viscous Flow over the Shuttle with Surface Catalytic Effects," AIAA Paper 83-1426, June 1983.

[8]Scott, C. D., "Effects on Nonequilibrium and Catalysis on Shuttle Heat Transfer," AIAA Paper 83-1485, June 1983.

[9]Stewart, D. A., Rakich, J. V., and Lanfranco, M. J., "Catalytic Surface Effects Experiment on the Space Shuttle," *Progress in Astronautics and Aeronautics: Thermophysics of Atmospheric Entry*, Vol. 82, edited by T. E. Horton, AIAA, New York, 1982, pp. 248–272.

[10]Rakich, J. V., Stewart, D. A., and Lanfranco, M. J., "Results of a Flight Experiment on the Catalytic Efficiency of the Space Shuttle Heat Shield," AIAA Paper 82-0944, June 1982.

[11]Kim, M. D., Bhutta, B. A., and Lewis, C. H., "Three-Dimensional Effects Upon Real Gas Flows Past the Space Shuttle," AIAA Paper 84-0225, Jan. 1984.

[12]Thareja, R. R., Szema, K. Y., and Lewis, C. H., "Viscous-Shock-Layer Predictions for Hypersonic Laminar or Turbulent Flows in Chemical Equilibrium over the Windward Surface of a Shuttle-Like Vehicle," AIAA Paper 82-0201, Jan. 1982.

[13]Thompson, R. A., "Three-Dimensional Viscous Shock Layer Applications for the Space Shuttle Orbiter," *Progress in Astronautics and Aeronautics: Thermophysical Aspects of Re-Entry Flows*, Vol. 103, edited by J. N. Moss and C. D. Scott, AIAA, New York, 1986, pp. 541–570.

[14]Moss, J. N. and Simmonds, A. L., "Galileo Probe Forebody Flowfield Predictions During Jupiter Entry," AIAA Paper 82-0874, June 1982.

[15]Thareja, R. R., Szema, K. Y., and Lewis, C. H., "Chemical Equilibrium Laminar or Turbulent Three-Dimensional Viscous Shock-Layer Flows," *Journal of Spacecraft and Rockets*, Vol. 20, Sept.–Oct. 1983, pp. 454–460.

[16]Swaminathan, S., Kim, M. D., and Lewis, C. H., "Three-Dimensional Nonequilibrium Viscous Shock-Layer Flows Over Complex Geometries," AIAA Paper 83-0212, Jan. 1983.

[17]Murray, A. L. and Lewis, C. H., "Hypersonic Three-Dimensional Viscous Shock-Layer Flows Over Blunt Bodies," *AIAA Journal*, Vol. 16, Dec. 1978, pp. 1279–1286.

[18]Szema, K. Y., Thareja, R. R., and Lewis, C. H., "Three-Dimensional Viscous Shock-Layer Flows Over Lifting Bodies at High Angle of Attack," AIAA Paper 81-1146, June 1981.

[19]Bird, R. B., Stewart, W. E., and Lightfoot, E. N., *Transport Phenomena*, Wiley, New York, 1960.

[20]Browne, W. G., "Thermodynamic Properties of Some Atoms and Atomic Ions," MSD Engineering Physics TM2, General Electric Co., Philadelphia, PA, 1962.

[21]Browne, W. G., "Thermodynamic Properties of Some Diatomic and Linear Polyatomic Molecules," MSD Engineering Physics TM3, General Electric Co., Philadelphia, PA, 1962.

[22]Browne, W. G., "Thermodynamic Properties of Some Diatoms and Diatomic Ions at High Temperature," MSD Advanced Aerospace Physics TM8, General Electric Co., Philadelphia, PA, May 1962.

[23]Armaly, B. F. and Sutton, K., "Viscosity of Multicomponent Partially Ionized Gas Mixtures Associated with Jovian Entry," *Progress in Astronautics and Aeronautics: Aerothermodynamics and Planetary Entry*, Vol. 77, edited by A. L. Crosbie, AIAA, New York, 1982.

[24]Mason, E. A. and Saxena, S. C., "Approximate Formula for the Thermal Conductivity of Gas Mixtures," *Physics of Fluids*, Vol. 1, No. 5, Sept.–Oct. 1958, p. 361.

[25]Yos, J. M., "Single Species Transport Properties for High-Temperature Gases," private communication to R. N. Gupta, Systems Division, AVCO, Wilmington, MA, June 1985.

[26]Armaly, B. F. and Sutton, K., "Thermal Conductivity of Partially Ionized Gas Mixtures," *Progress in Astronautics and Aeronautics: Thermophysics of Atmospheric Entry*, Vol. 82, edited by T. E. Horton, AIAA, New York, 1982.

[27]Davis, R. T., "Hypersonic Flow of a Chemically Reacting Binary Mixture Past a Blunt Body," AIAA Paper 70-805, July 1970.

[28]Blottner, F. G., Johnson, M., and Ellis, M., "Chemically Reacting Viscous-Flow Program for Multi-component Gas Mixtures," Sandia National Lab., Albuquerque, NM, Rept. SC-RR-70-754, Dec. 1971.

[29]Zoby, E. V., Gupta, R. N., and Simmonds, A. L., "Temperature-Dependent Reaction Rate Expressions for Oxygen Recombination," *Progress in Astronautics and Aeronautics: Thermal Design of Aeroassisted Orbital Transfer Vehicles*, Vol. 96, edited by H. F. Nelson, AIAA, New York, 1985, pp. 445–465.

[30]Weilmeunster, K. J. and Hamilton, H. H., II, "Calculations of Inviscid Flow over Shuttle-Like Vehicles at High Angles of Attack and Comparisons With Experimental Data," NASA TP-2103, May 1983.

[31]Throckmorton, D. A., "Benchmark Determination of Shuttle Orbiter Entry Aerodynamic Heat-Transfer Data," *Journal of Spacecraft and Rockets*, Vol. 20, May–June 1983, pp. 219–224.

[32]Zoby, E. V., "Analysis of STS-2 Experimental Heating Rates and Transition Data," *Journal of Spacecraft and Rockets*, Vol. 20, May–June 1983, pp. 232–237.

[33]Hamilton, H. H., II, "Approximate Method of Predicting Heating on the Windward Side of Space Shuttle Orbiter and Comparisons with Flight Data," AIAA Paper 82-0823, June 1982.